Tribology International 210 (2025) 110772

Contents lists available at ScienceDirect

Tribology International

journal homepage: www.elsevier.com/locate/triboint

Full Length Article

Impact of the tire/road local contact area on tire friction, with a novel approach based on Greenwood–Williamson theory and validation in both laboratory and outdoor racing environments

Flavio Farroni [a], Raffaele Stefanelli [a,*], Guido Napolitano Dell'Annunziata [a], Francesco Timpone [a]

[a] University of Naples Federico II, Department of Industrial Engineering, Via Claudio, 21, Naples, 80125, Italy

ARTICLE INFO

Keywords:
Contact modeling
Road roughness characterization
Viscoelasticity
Tire friction

ABSTRACT

Tire-road interaction involves complex phenomena related to contact modeling and the evaluation of the friction coefficient in different conditions. Over the years, many approaches have been followed to develop physical models capable of considering all the relevant parameters, such as viscoelastic properties, road roughness and tire conditions. In this scenario, contact modeling is a fundamental topic as the effective contact area, when the tire is in contact with the road, is smaller than the nominal area due to the indentation of the rubber on road asperities. This paper presents an extended version of the Greenwood–Williamson contact model able to evaluate the ratio between the real contact area and the nominal one (A_c/A_0), exploiting a complete non-destructive characterization procedure for the evaluation of the tire tread viscoelastic properties and an innovative method to estimate the road roughness descriptors.

1. Introduction

A crucial role in understanding the complex phenomena governing tire-road interactions is played by contact mechanics and friction [1–3]. When friction occurs, energy dissipation takes place, and in micro-contact regions subject to very high stresses, it can trigger micro-fractures and subsequent surface wear [4–6]. An essential aspect of the tire-road interaction process is about how the rubber penetrates the road asperities during contact [7–9]. Since the area engaged by the rubber during contact with the asphalt depends on the level of indentation into the road profile, an effective way to assess its influence on the friction coefficient is by analyzing the ratio of the actual contact area (A_c) to the nominal contact area (A_0), the latter representing the area that the rubber would cover if it conformed perfectly to all road asperities.

To study these effects, the proposed research activity presents a robust approach to predicting the A_c/A_0 ratio and its relationship with experimental friction coefficient in both indoor and outdoor environments. This is achieved by integrating non-destructive characterization of tire viscoelasticity and an innovative method for analyzing road roughness.

Numerous authors have provided valuable insights into determining contact theories and, by extension, the level of indentation of the rubber with the surface texture. The foundation of modern contact mechanics can be traced back to Heinrich Hertz's work in 1882 [10]. Hertz's contribution introduced a widely used analytical solution for the contact of two elastic axisymmetric parabolic structures. He provides a precise approximation for various contact scenarios, including interactions between two spheres. Moreover, by assuming an infinite radius of curvature for one of the bodies, the model naturally extends to analyze the contact between a sphere and an elastic half-space [11,12]. Under the assumption of a quadratic pressure distribution, this framework enables the calculation of vertical displacement during contact, indentation of the elastic half-space, contact radius, and real contact area, given the sphere's radius and the elastic modulus of the half-space [13].

Incorporating surface roughness into contact models presents considerable challenges due to its complexity and randomness [14]. Despite these limitations, researchers have developed numerous models to predict contact behavior for rough real surfaces. Statistical models, in particular, have gained prominence by conceptualizing the real surface as a statistical distribution of asperities [15]. In such models, the total load is computed as the summation of individual loads on contacting asperities, allowing for the application of Hertz contact theory to each contact region corresponding to the asperities.

* Corresponding author.
E-mail addresses: flavio.farroni@unina.it (F. Farroni), raffaele.stefanelli@unina.it (R. Stefanelli), guido.napolitanodellannunziata@unina.it (G. Napolitano Dell'Annunziata), francesco.timpone@unina.it (F. Timpone).

https://doi.org/10.1016/j.triboint.2025.110772
Received 12 March 2025; Received in revised form 29 April 2025; Accepted 3 May 2025
Available online 21 May 2025

Bowden and Tabor in 1939 highlighted the importance of surface roughness as a fundamental factor to consider in contact mechanics [16]. Their investigations revealed a significant difference between the real and nominal contact areas of frictional partners. The presence of surface curvature or roughness often confines contact to microscopic areas near surface peaks or asperities, resulting in elevated contact stresses that can precipitate failure or yielding within the contact regions [17].

In the study of contact among real rough surfaces, Archard's works in the 1950s [18,19] highlighted the discrepancy between the predictions of the Hertzian theory and experimental observations of a linear relationship between contact area and applied load. To address it, he proposed a generalized model considering the contact between rough surfaces, incorporating multiple levels of asperities leading to increasingly accurate approximations to the linear relationship (between contact area and applied load) as more stages were considered. This multi-contact theory extends Hertzian contact theory to account for multiple contact areas between a rigid flat surface and a deformable flat surface containing a series of spherical asperities uniformly distributed along the z axis. Furthermore, Archard's findings underlined the presence of an infinite sequence of length scales within surface profiles. This causes difficulty in defining individual asperities, as their characterization depends on the chosen scale of observation. While larger sampling intervals reveal only the most prominent asperities, finer intervals expose many smaller features.

The generalization of the Hertz solution to arbitrarily shaped bodies is attributed to Ian Sneddon with his paper published in 1965 [20]. Sneddon's work explores the interaction between a rigid body of arbitrary shape and a linearly elastic half-space, providing solutions applicable to various punch shapes. However, these classical solutions present a nonlinear relationship between contact area and applied force and they are based on the simplified hypotheses of non-adhesive contact, where no tensile forces are allowed to occur within the contact area.

Greenwood and Williamson (GW) [21] and Bush [22] employed statistical methods to describe surface topography and built models able to evaluate the real contact area. In particular, their works revealed that in rough materials, the real contact area is generally proportional to the normal force. Greenwood and Williamson proposed their contact model in which the rough nature of a surface is described as a distribution of spherically shaped asperities, all with the same radius of curvature but varying in height according to a specified probability density function. Bush et al. introduced a slightly different model that departed from the spherical asperities assumed in the GW model, modeling the individual asperities with a paraboloidal shape with the same principal curvature. Jackson and Green offered a comprehensive and modern closed-form derivation of the classical Greenwood–Williamson model to bypass the difficulties of numerical integrations [23]. Their formulation offers a useful analytical reference for Hertzian-based contact models with spherical asperities and Gaussian height distributions.

To address the role of adhesion in contact mechanics, the Johnson-Kendall-Roberts (JKR) model and the Derjaguin-Muller-Toporov (DMT) model were developed. The presence of adhesion between surfaces becomes particularly pronounced in softer materials like elastomers, where attractive forces between surfaces play a significant role and the attraction forces explain why a mechanical load is necessary to separate two solid bodies in intimate contact, especially under light loading conditions [24]. The mentioned models incorporate adhesive forces into the contact analysis, which are primarily based on solid–solid (van der Waals) interactions. In 1971, Johnson, Kendall, and Roberts proposed their solution for adhesive contact, considering short-range attraction forces within the contact area [25]. Shortly after, in 1975, Derjaguin and colleagues proposed the DMT model, which adds adhesive pressures outside the contact region [26]. Although in different regions, both these models introduce a surface adhesive energy term in addition to the stored elastic energy and yield the same result as the Hertz model in the absence of adhesion.

Initially perceived as competing theories, the debate between the JKR and DMT models was resolved by recognizing that, while both correctly represent adhesive contact, their applicability depends on the material properties. Specifically, the DMT model is suitable for stiff samples with low adhesion, while the JKR model is applicable to softer samples with higher adhesion [27,28]. Maugis [29] demonstrated the transition from DMT to JKR behavior by incorporating adhesive forces both inside and outside the contact zone. His work reconciled these models offering a semi-analytical parametric solution to the adhesive contact problem. It should be underlined that in all these models, a nonlinear relationship between the normal load and contact area is found as well.

In the past few decades, contact mechanics research has advanced considerably, integrating more sophisticated experimental tools and accurate numerical simulations. Persson developed a different approach to contact mechanics: it accounts that for small squeezing force the real contact area A_c is proportional to the load F_N, while as F_N increases A_c approaches A_0 in a continuous manner [30,31].

Le Gal and Klüppel introduced a semi-analytical method to accurately describe the regions of a rough surface where actual contact occurs. This approach is crucial for calculating contact parameters that are predominantly influenced by the largest length scales of the surface profile [5], such as pressure distribution and friction. With a similar approach, Heinrich tends to emphasize the understanding of the interplay between viscoelastic properties and surface roughness at multiple scales. His theory integrates both the adhesive and hysteretic components of friction, examining how surface asperities deform elastomers and influence real contact areas [32].

Müser investigated the role of non-linearity and non-locality in interactions involving both soft and hard materials [33]. He also provided significant insights into how micro-scale surface morphology dictates the contact area of solids and the forces they exert on one another.

Starting from the GW contact theory for its versatility and generalizability, this study presents a physical-analytical model to predict the local tire-road contact area in both outdoor and racing contexts, as well as in controlled indoor environments. The main innovations are based on the introduction of a non-destructive approach to characterize the viscoelastic properties of the tire using an innovative device named VESevo (Viscoelasticity Evaluation System evolved), combined with a specific road roughness characterization process, which allows for the extraction of the main texture indicators. The proposed approach enables the simulation of the real-to-nominal contact area ratio A_c/A_0, which shows a direct correlation with the friction coefficient. By scanning the road surface, evaluating tire viscoelastic properties, assessing various operating conditions, and carefully processing input parameters, this study demonstrates that an indentation-based local contact model can effectively capture the physical mechanisms underlying tire-road interaction. By establishing a clear correlation between the A_c/A_0 ratio and the experimental friction coefficient, the model gives the possibility to predict the friction behavior among the various surfaces before any experimental tests are performed. Furthermore, unlike traditional approaches, which often require surface-specific calibration or are limited to controlled environments, this model has been extended and validated across a remarkably different range of surfaces and condition, including both controlled indoor conditions and real-world outdoor scenarios. It demonstrates consistent performance on standard road samples or racing tracks as well as unconventional surfaces, such as sandpaper, without requiring adjustments to the methodology. This highlights the model's robustness and practical applicability, providing reliable insights into relative friction levels across different surfaces and operational conditions. It also provides a fast and effective method for assessing tire performance, saving time and resources in testing and design processes, particularly for high-performance and racing applications. For these reasons, the model's applicability across different

scenarios represents a significant advancement in the state of the art, offering both versatility and robustness.

This paper is organized as follows: Sections 2 and 3 provide the input details for the contact model. Specifically, Section 2 focuses on road roughness characterization, describing both indoor and outdoor environments along with the methods used for data acquisition. Section 3 discusses the viscoelastic properties of the rubber compound considered in this research, highlighting their evaluation through a non-destructive procedure using the VESevo device. Section 4 introduces the contact model used to compute the ratio between the real and nominal contact areas, emphasizing its dependence on surface roughness and tire operating conditions. Finally, Section 5 provides a detailed analysis of friction behavior, correlating experimental friction values with the simulated A_c/A_0 ratios for both indoor and outdoor environments. This is followed by a final discussion in Section 6 and the conclusions in Section 7.

2. Road roughness characterization

Road roughness refers to deviations in the pavement surface height relative to a reference plane and is commonly measured along a single line profile or across multiple parallel profiles, which can be compiled into surface maps [34]. To support the case study presented here, a high-resolution profilometer was used to scan a variety of surfaces, providing detailed roughness profiles essential for determining the A_c/A_0 ratio. Specifically, several specimens were analyzed under controlled indoor conditions; the selected surfaces varied in both chemical composition and indicative petrology (limestone, sandstone, granite, porphyry, and basalt). Beyond asphalt samples, sandpapers of different grit sizes were also scanned to simulate additional interaction scenarios with rubber, thus allowing the evaluation of a broader spectrum of surface roughness conditions. Moreover a range of outdoor tracks with distinct characteristics was investigated as well.

Fig. 1 shows the 2D roughness profiles of both road specimens and sandpapers, clearly illustrating the differences between the surfaces. Specifically, the profiles differ in terms of the distribution of peaks and valleys, the height and spacing of the peaks, and the overall roughness patterns, highlighting the distinct road roughness characteristics of each surface.

This analysis enabled consideration of different surfaces, challenging the model with unconventional scenarios, such as tire-sandpaper interactions similarly to what happens with flat track [35].

On the other side, five different tracks were scanned with the aim of running various simulations not only for indoor environments but also for outdoor ones. Through this approach, the model's adaptability and coherence were evaluated across a broader spectrum of surface characteristics. A representation of an acquired profile as example for each track is shown in Fig. 2.

A wide range of techniques can be used to investigate the texture of asphalt for different surface topologies. In practice, statistical parameters are often combined with spectral analysis tools to describe the road surface [36–38]. Roughness parameters are generally classified into three categories based on their function: amplitude parameters, spacing parameters, and hybrid parameters. Amplitude parameters capture vertical attributes of the surface, critical for defining its topography. One of the most prominent and widely utilized among these is the center line average Ra, a general roughness indicator used for quality assessments:

$$Ra = \frac{1}{L}\int_0^L |z(x) - m| dx \tag{1}$$

where L is the sampling length of the profile, $z(x)$ is a generic surface profile and m is the mean of the heights. By contrast, spacing parameters convey information about horizontal features of the surface, such as the wavelength λ [39,40]:

$$\lambda = 2\pi \frac{\int_0^L |z(x) - m| dx}{\int_0^L |z'(x)| dx} \tag{2}$$

where $z'(x)$ is the slope of the profile.

To achieve a more holistic description of the captured profile, hybrid parameters are also considered. These merge characteristics of both amplitude and spacing, and thus any modifications to either vertical or horizontal measures can influence them. Typical examples include surface slope and curvature, both of which play a significant role in determining tribological properties.

When examining the texture of tarmac, it is necessary to analyze both the macro-roughness and micro-roughness. The former refers to more pronounced, long-wavelength irregularities, while the latter arises from shorter-wavelength variations, encompassing asperities (local maxima) and valleys (local minima) with varying amplitude and spacing [41].

In the context of friction theory, these two scales play a crucial role in determining the interaction between surfaces. The macro-roughness primarily affects the overall contact area and load distribution, while the micro-roughness influences local adhesion and shear forces, as described in two-scale friction models [42]. These models highlight how surface texture at both scales contributes to tire grip and overall frictional behavior.

2.1. Innovative roughness data processing

The approach to the road roughness data processing presented in this work is based on geometric aspects of the surface texture, with the aim to overcome the limits of the spectral analysis, especially regarding the micro-scale. The innovation of the approach lies in the analytical analysis of the roughness profile: the presented approach introduces a structured methodology for extracting micro-roughness profiles directly from experimental macro-scale surface data. By isolating only the local maxima (which are physically relevant to tire-road contact), removing macro-slope effects and analyzing each micro-profile individually, the method allows for a more representative and physically grounded characterization of the actual asperities involved in contact. This contrasts with more traditional frequency-domain spectral analyses, which can suffer from ambiguities. Specifically, for what concerns the Height Difference Correlation Function (HDCF), described in detail in the next paragraph, it becomes difficult to accurately identify key points such as the slope change, which is critical for determining road texture parameters at the micro-scale. Thus, the analysis of both macro and micro scale is a crucial topic for the tire-road interaction field [43].

In particular, according to the main road parameters previously presented, once the macro profile is acquired with a specific texture scanner, it is possible to evaluate the main macro roughness descriptors which give information about the global road roughness. Differently, by isolating the roughness of the single asperities, it is possible to analyze the micro-roughness of the acquired profile. The developed approach is based on the fact that the tire-road contact occurs on the peaks of the road profile [44]. For this reason, the aim is to detect the peaks from the acquired profile and subsequently extract micro-profiles of a specified width along the X-direction, defined as the direction in which the roughness profile was acquired. The steps followed to obtain the final micro-roughness profiles are presented in Fig. 3.

A step-by-step schematic representation of the procedure to obtain the final micro-roughness profiles is outlined below:

1. Acquisition of road roughness profile
2. Detection of local maxima by isolating only the peaks that contribute to the tire-road interaction
3. Removal of the underlying macro-slope effect to isolate individual rocks
4. Application of analytical formulations to obtain the micro-roughness indicators

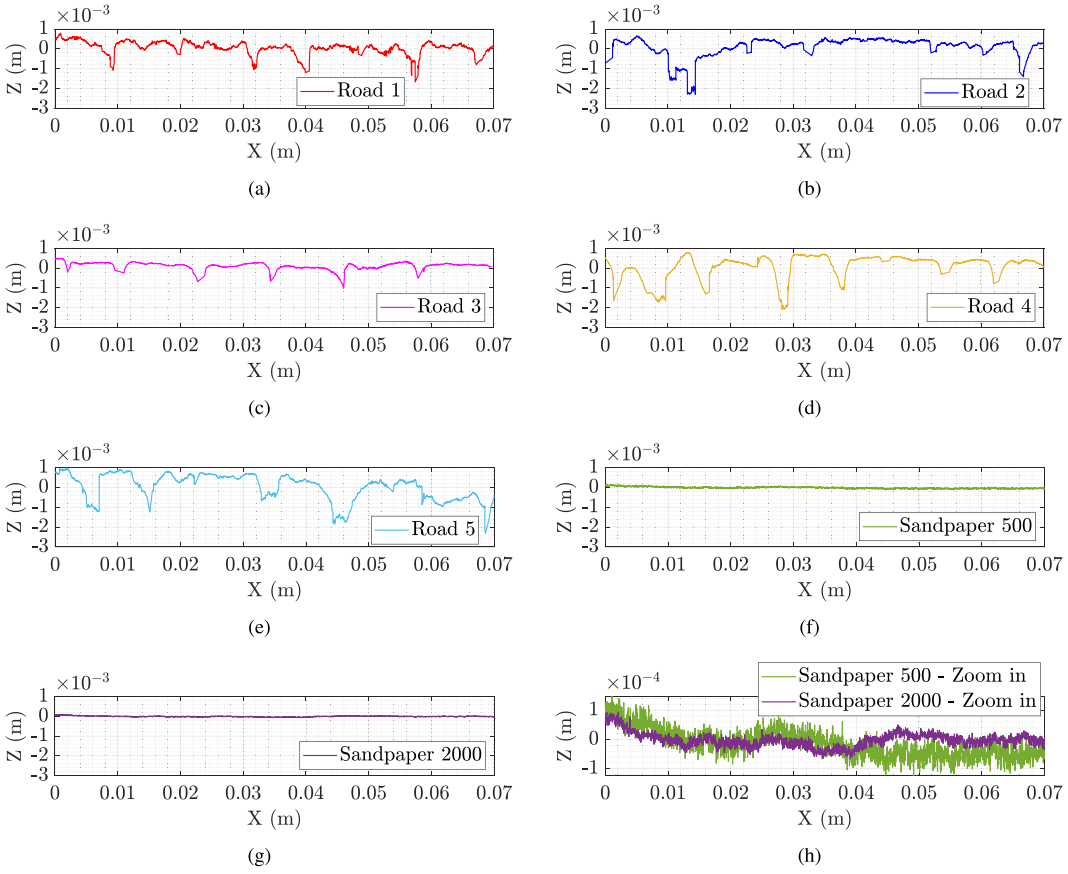

Fig. 1. Road specimens and sandpapers 2D laser scan: (a) Road specimen 1, (b) Road specimen 2, (c) Road specimen 3, (d) Road specimen 4, (e) Road specimen 5, (f) Sandpaper grit 500, (g) Sandpaper grit 2000, (h) Zoom-in for both sandpapers.

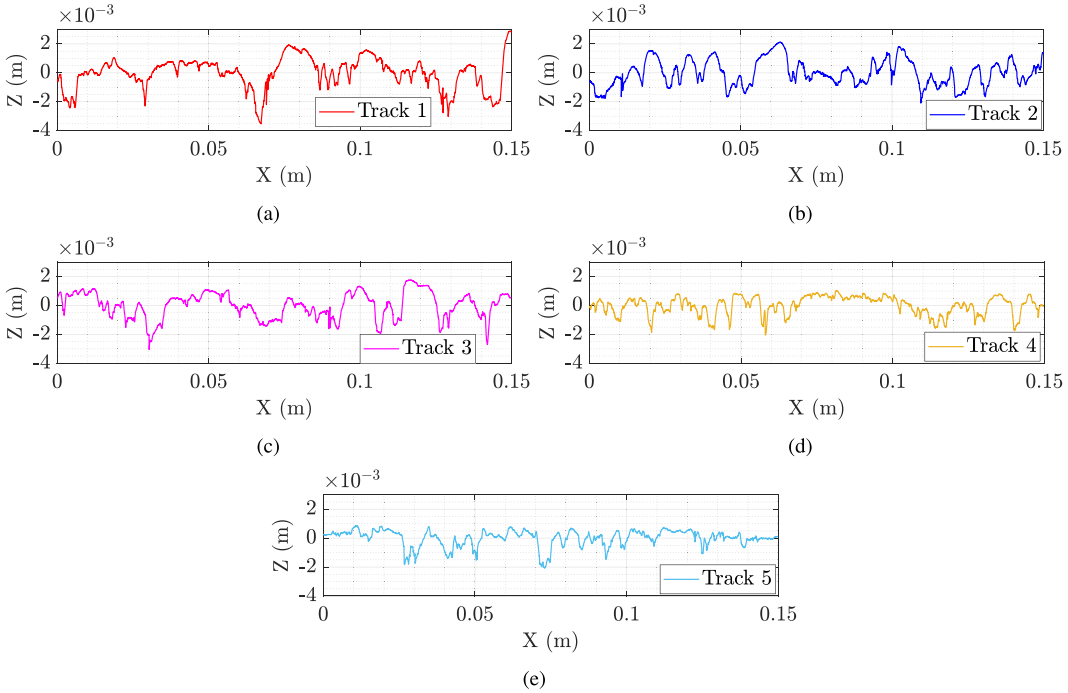

Fig. 2. Tracks 2D laser scan: (a) Track 1, (b) Track 2, (c) Track 3, (d) Track 4, (e) Track 5.

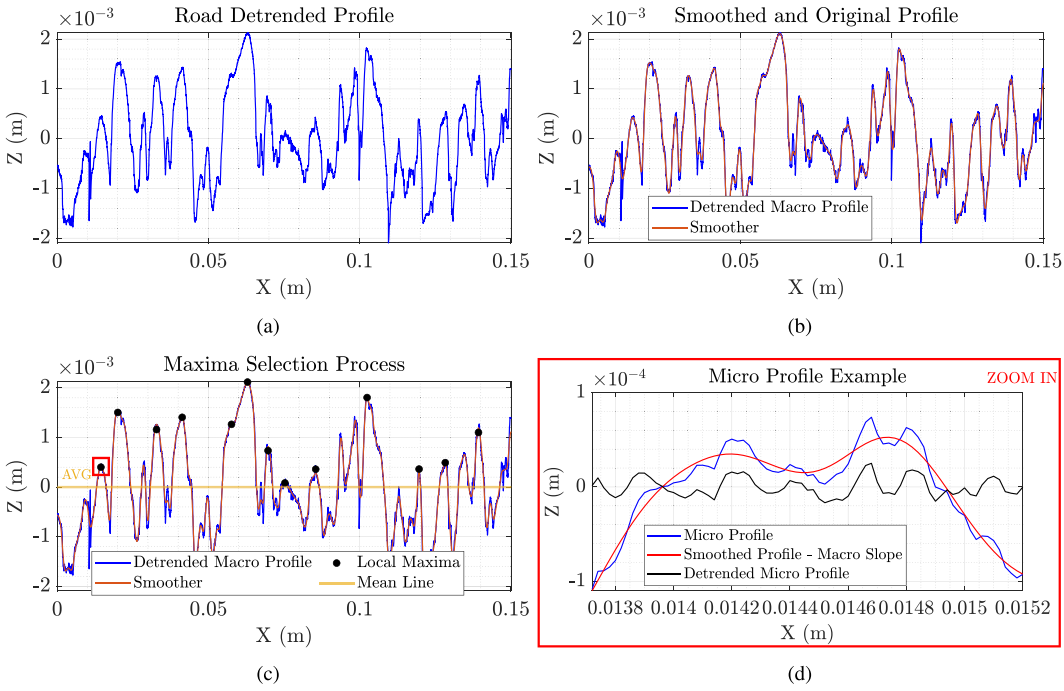

Fig. 3. Micro-roughness profiles detection: (a) Experimentally acquired macro roughness profile, (b) Application of the smoother on the macro profile, (c) Local maxima identification, (d) Example of an extracted micro profile.

Table 1
Roughness indicators for the indoor road specimens.

Variables	Road 1	Road 2	Road 3	Road 4	Road 5
λ_{Macro} (m)	2.63E−03	3.58E−03	4.13E−03	4.13E−03	3.70E−03
λ_{micro} (m)	7.64E−05	7.06E−05	7.02E−05	7.04E−05	7.39E−05
Ra_{Macro} (m)	5.32E−04	5.10E−04	5.22E−04	5.25E−04	5.32E−04
Ra_{micro} (m)	1.52E−05	9.63E−06	8.97E−06	8.00E−06	8.66E−06
Ku (–)	5.24E+00	6.52E+00	7.21E+00	5.34E+00	5.56E+00
Sk (–)	−1.42E+00	−1.86E+00	−1.90E+00	−1.50E+00	−1.48E+00
MPD (m)	1.28E−03	8.61E−04	1.10E−03	1.17E−03	1.11E−03

Table 2
Roughness indicators for the outdoor tracks.

Variables	Track 1	Track 2	Track 3	Track 4	Track 5
λ_{Macro} (m)	5.84E−03	5.52E−03	6.02E−03	4.13E−03	3.95E−03
λ_{micro} (m)	1.56E−04	1.84E−04	1.59E−04	1.82E−04	1.94E−04
Ra_{Macro} (m)	8.06E−04	7.43E−04	7.36E−04	5.07E−04	4.16E−04
Ra_{micro} (m)	1.06E−05	1.21E−05	1.12E−05	1.10E−05	1.25E−05
Ku (–)	3.60E+00	2.36E+00	2.64E+00	2.94E+00	4.74E+00
Sk (–)	−5.13E−01	2.30E−01	−4.08E−01	−8.05E−01	−1.36E+00
MPD (m)	2.88E−03	2.13E−03	1.78E−03	1.01E−03	8.76E−04

It is thus clear that, to study the effect of the single asperities, the first step consists of the local maxima detection: to perform this, a smoother is applied to the macro profile in order to identify all the summits of the road profiles. To select only the peaks that contribute to tire-road contact, all the ones under the mean line of the profile have been neglected.

By isolating the profiles thus extracted, it can be observed that they are affected by the slope of the underneath road macro profile, which needs to be removed to have the final micro profile representative of the single rock. The various micro profiles are then used as input for the analytical formulation of the main descriptors and the average value is the final representation of the micro roughness indicators.

Some of the road roughness indicators related to both the road specimens and the tracks considered for this research activity in terms of roughness are reported in Tables 1 and 2, in which Ku stays for Kurtosis, Sk for Skewness and MPD for Mean Penetration Depth.

The two-scale roughness indicators presented in Tables 1 and 2 serve a dual purpose: to provide a comprehensive characterization of the road surface morphology at both macro and micro scales and to supply key inputs to the contact model. In particular, the roughness wavelength is directly used to calculate the A_c/A_0 ratio.

2.2. Height difference correlation function

The Height Difference Correlation Function plays an important role in evaluating other road roughness parameters. Some of the indicators derived from the HDCF are necessary road inputs for the contact model presented in this paper, as they directly contribute to the analytical formulation of the same. This function, denoted $C_z(\lambda)$, represents the mean square height fluctuations of the surface relative to a horizontal length scale λ [45]. In situations where two scaling regimes are required, one for macro roughness and another for micro roughness, the horizontal ($\xi_\parallel$) and vertical ($\xi_\perp$) cut-off lengths, along with the Hurst exponent (H), are introduced. Under these conditions, $C_z(\lambda)$ is described by [5,6,46]:

$$C_z(\lambda) = \xi_\perp^2 \left(\frac{\lambda}{\xi_\parallel}\right)^{2H_M} \quad for\ \lambda_x < \lambda < \xi_\parallel \tag{3}$$

$$C_z(\lambda) = \xi_\perp^2 \left(\frac{\lambda_x}{\xi_\parallel}\right)^{2H_M} \left(\frac{\lambda}{\lambda_x}\right)^{2H_m} \quad for\ \lambda < \lambda_x \tag{4}$$

where λ_x denotes the point at which the two scaling regimes intersect, and the exponents H_m and H_M respectively capture the micro and macro roughness behavior.

The representation of the HDC function for both the indoor road specimens and the various tracks considered for this research activity is depicted in Fig. 4.

3. Tire tread viscoelastic properties evaluation from innovative non-destructive testing

Understanding the viscoelastic behavior of tire tread is essential for analyzing tire-road interaction, as it provides valuable insights

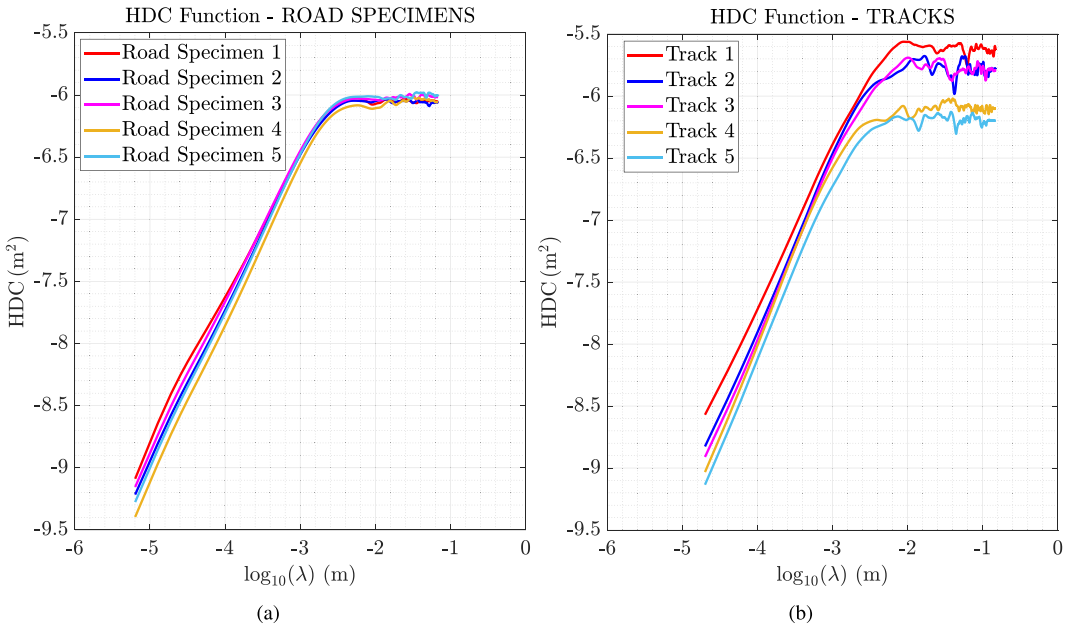

Fig. 4. HDC functions of the various surfaces: (a) HDC functions of the road specimens, (b) HDC functions of the tracks.

that complement other critical factors and contribute to optimizing vehicle performance. Viscoelastic materials exhibit characteristics of both elastic solids and viscous fluids [47,48]. The storage modulus, energy dissipation, and hysteresis of a viscoelastic material vary in response to two key factors: the frequency of the applied force and temperature, which influence the rubber in opposite ways [49]. At a constant temperature, an increase in stress frequency causes the polymer to adopt a glassy state. In contrast, when the temperature rises while the stress frequency remains unchanged, the material softens and behaves like rubber [50,51]. These effects stem from the interplay between molecular motion and strain rate. When the strain rate exceeds the speed at which molecular chains can rearrange within the polymer structure, the material behaves as a rigid glassy solid. In contrast, if the strain rate is lower than the molecular movement speed, the material displays rubbery characteristics. At extremely low temperatures, rubber remains highly rigid; however, upon reaching a critical transition temperature, the molecular bonds within the polymer network begin to break, causing the rubber to soften significantly at higher temperatures. The temperature at which intermolecular bonds break down is called transition temperature and it is denoted as T_g [52].

Determining the viscoelastic properties of the tire tread, affected by both rubber temperature and the frequency of bitumen asperity interactions, is crucial for modeling contact mechanics and estimating the upper limit of the local friction coefficient. Dynamic Mechanical Analysis (DMA) [53] is a commonly used destructive testing method for characterizing viscoelastic behavior, allowing for the assessment of hysteresis in accordance with the Time-Temperature Superposition Principle [54]. This technique requires polymer specimens of precise dimensions and relies on complex, costly equipment to analyze generic compound samples. Additionally, as a destructive method, it is unsuitable for tire tread analysis without causing irreversible damage. This limitation creates a big challenge for motorsport racing teams, as those tires cannot be subjected to destructive testing. Indeed, due to strict constraints imposed by regulations and tire supplier, which prohibit any form of tire destruction, the ability to access viscoelastic data in such contexts is highly limited. In this context, the development and use of a non-destructive testing procedure capable of extracting the viscoelastic master curve of rubber represents a substantial advancement, enabling effective integration of experimental data into predictive modeling and vehicle performance optimization workflows.

Fig. 5. VESevo device in operation for testing a high-performance tire.

The VESevo is a portable device (Fig. 5) developed by the Vehicle Dynamics research group at the University of Naples Federico II. It enables non-destructive characterization of tire tread viscoelastic properties [55,56]. This innovative approach to assessing compound viscoelasticity serves as a key input for the physical-analytical model proposed in this study. At its core, the device features a steel rod equipped with a semi-spherical indenter that is free to bounce on the tire tread surface while sliding within a specially designed guide. The rod consistently starts from the same initial position for each test and its displacement is captured by an optical sensor with an exceptionally high frequency response. This setup allows for a large number of tests to be conducted in a short time with high repeatability, providing viscoelastic data that directly contribute to the model for predicting the A_c/A_0 ratio.

The objective of the test is to obtain the rebound curves of the VESevo rod on the rubber sample for different thermal levels. Fig. 6 illustrates how the shape of the rebounds changes with temperature.

The analysis of the rebound curves was conducted by separately examining the indenter's free-fall phase and its contact phase with the rubber surface. This approach allowed for the estimation of mechanical

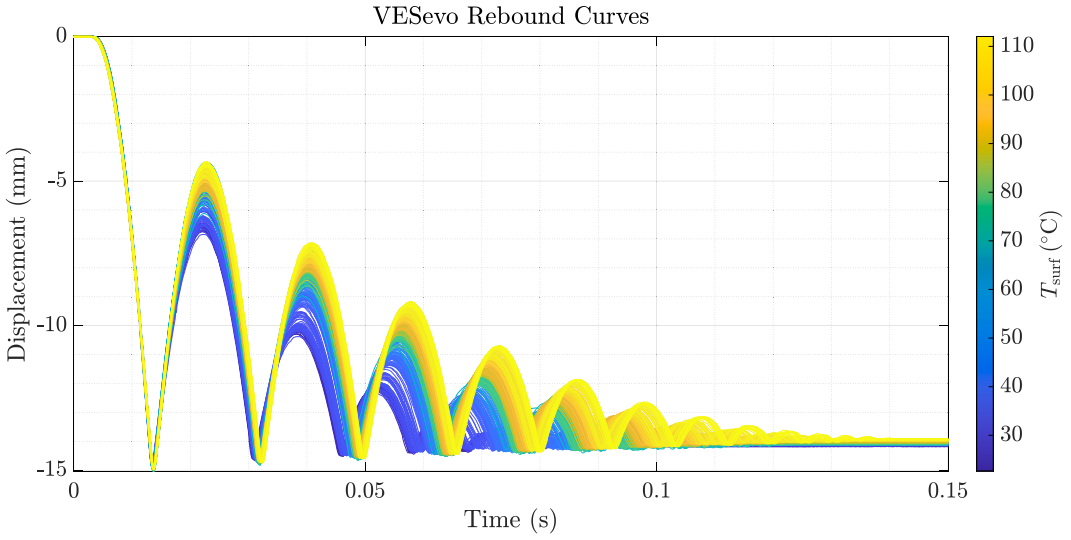

Fig. 6. VESevo rebound curves variation according to the temperature (in the colorbar on the right).

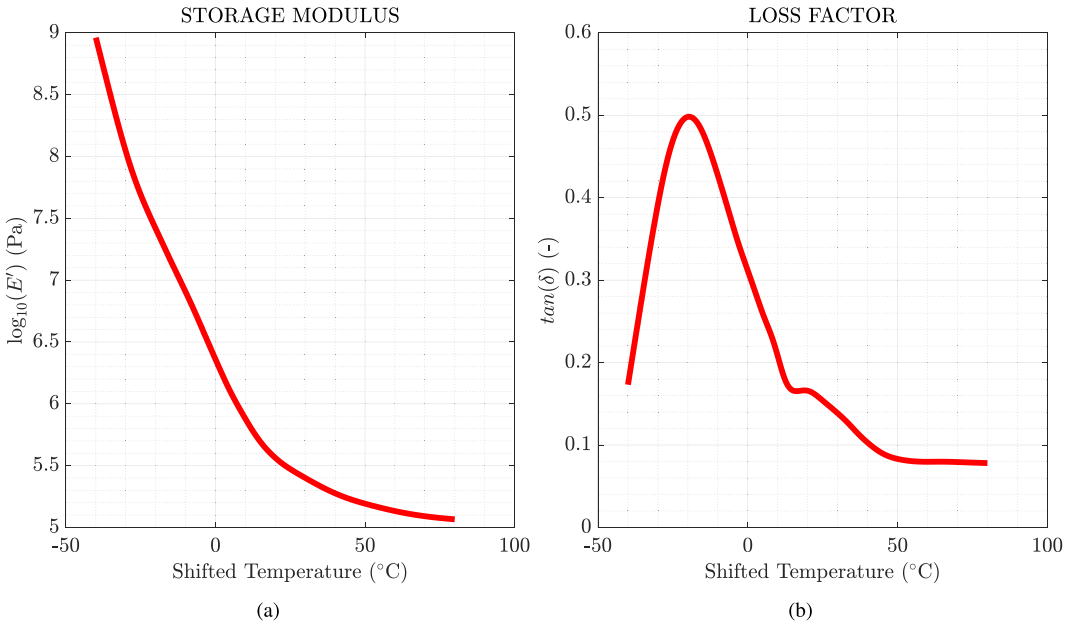

Fig. 7. Viscoelastic properties of the reference compound: (a) Storage modulus, (b) Loss factor.

properties, such as the stiffness and damping characteristics of both the instrumented indenter and the bulk rubber sample. These parameters were then utilized to generate the viscoelastic master curves of the reference compound through a proprietary algorithm [57].

Another crucial factor is the dependence of viscoelastic properties on both frequency and temperature, as previously discussed. To address this, the methodology establishes the master curve at a reference frequency and adjusts it according to the temperature variations. As a result, instead of evaluating the curve at the actual measured temperature, it is assessed at an equivalent temperature that corresponds to the frequency of interest. This concept, known as shifted temperature, is implemented using the Williams-Landel-Ferry (WLF) equation [58].

The viscoelastic properties of the reference compound used in this research, for both indoor and outdoor environments, were evaluated using the VESevo device and are reported in Fig. 7.

4. Contact model developed according to the Greenwood-Williamson theory

The Greenwood and Williamson model was developed in 1966 [21] and considers the contact between two elastic bodies: a plane (smooth surface) and a nominally flat one (rough surface), where the distance between the first and the reference plane of the second is given by the separation d, as depicted in Fig. 8.

To solve this contact problem within the framework of GW theory, the rough surface is modeled to be covered with a large number of asperities, which are assumed to be spherical, at least near their summits, with the same radius R, and their heights vary following a continuous distribution $\phi(z)$, as it can be depicted in Fig. 9. According to [59], the spheres are assigned a fixed radius of curvature defined by:

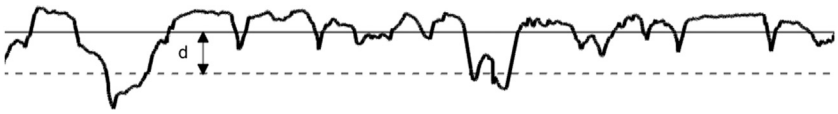

Fig. 8. Contact between a plane and a nominally flat surface. The load is supported by those asperities (shaded) whose heights are greater than d.

Fig. 9. Continuous distribution $\phi(z)$ associated to the rough surface in the Greenwood Williamson framework.

$$R = {\xi_{\parallel}}^2/(4\pi\xi_{\perp}) \tag{5}$$

In this context, contact occurs at any asperity whose initial height exceeds d. The contact between an asperity and a smooth counter-surface is described within the framework of Hertzian contact theory. This allows for the evaluation of the total contact area resulting from the interaction between individual asperities and a flat surface. In this way, it is possible to obtain the real contact area A_c, which is smaller than the nominal one A_0 due to the roughness effect.

The theory of Greenwood and Williamson was extended by Klüppel, Heinrich and Le Gal to describe the contact mechanism during tire-road interaction accounting for the viscoelastic characterization of the rubber material and the statistical description of the road roughness [5,32].

The implemented model for this research activity is based on the extension of the Greenwood–Williamson (GW) model by Klüppel and Heinrich to account for rubber friction on rough surfaces [6]. The mentioned model provides the A_c/A_0 ratio for the contact between a viscoelastic material, the tire, and a rough surface. The model takes as input the tire's operating conditions, including sliding velocity, the surface temperature of the rubber and the contact pressure between the two contacting bodies. Although various methods exist to estimate rough surface contact parameters [60], the approach adopted in this work follows [59,61], as it defines these parameters consistently with the specific extension of the GW model presented by Klüppel and Heinrich.

Together with the A_c/A_0 ratio, an essential quantity is represented be the so-called minimal contact length scale λ_{min} which is obtained through an energy based condition of elastic contact [62]. In particular, λ_{min} is evaluated as:

$$\frac{\lambda_{min}}{\xi_{\parallel}} \approx \left[\left(\frac{\lambda_x}{\xi_{\parallel}} \right)^{3(D_m - D_M)} \frac{0.09\pi s^{3/2}\xi_{\perp} F_0(t)|E^*(2\pi v/\lambda_{min})|\tilde{n}_s}{\xi_{\parallel}|E^*(2\pi v/\xi_{\parallel})|F_{3/2}(t_s)} \right]^{\frac{1}{3D_m - 6}} \tag{6}$$

where:

- $\xi_{\parallel}$ corresponds to the largest wavelength found in the road profile. In particular, the roughness wavelength is directly used to calculate the correlation length $\xi_{\parallel}$, which enters the evaluation of the minimum contact length λ_{min} and ultimately influences the computed A_c/A_0 ratio. Rather than estimating $\xi_{\parallel}$ from the HDCF, an approach which may suffer from experimental uncertainties, it is computed analytically from the wavelength. This choice is consistent with the theoretical framework introduced by Klüppel and Heinrich and later implemented by Le Gal;
- $\xi_{\perp}$ is defined by $\xi_{\perp}^2 = C_z(\xi_{\parallel})$, i.e., it is the square root of the HDC function evaluated at $\xi_{\parallel}$;

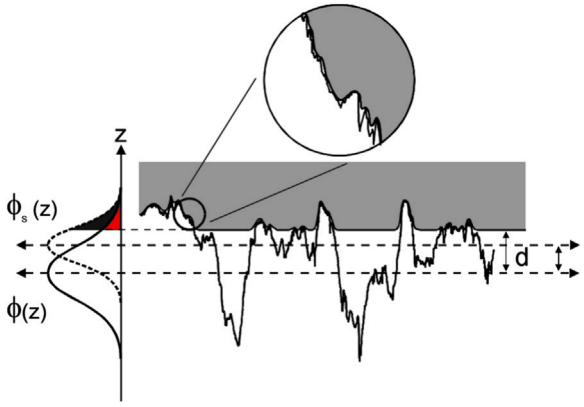

Fig. 10. Height distribution $\Phi(z)$ and summit height distribution $\Phi_s(z)$ associated to the rough surface.

- v represents the speed at which the rubber slides over the rough substrate;
- $E^*(\frac{2\pi v}{\lambda_{min}})$ and $E^*(\frac{2\pi v}{\xi_{\parallel}})$ represent the tire rubber's dynamic modulus evaluated at the frequencies $\frac{2\pi v}{\lambda_{min}}$ and $\frac{2\pi v}{\xi_{\parallel}}$. The temperature dependence is captured via the time–temperature superposition principle [51]. Indeed, viscoelastic modulus interpolation was cross-validated against master curve data to ensure consistency;
- s is an affine parameter evaluated from a numerical optimization process. It maps the substrate's original height distribution $\Phi(z)$, to the summit height distribution $\Phi_s(z)$ of macroscopic asperities, using:

$$z_s = z_{max} + \frac{z - z_{max}}{s} \tag{7}$$

where z_{max} is the maximum substrate height. Fig. 10 shows an example of both $\Phi(z)$ and $\Phi_s(z)$ distributions of a rough profile. In particular, s is obtained through a non-linear least squares minimization with a procedure that fits the statistical distribution of summits extracted from surface profiles to a Gaussian probability density function (pdf), by minimizing the error between the empirical summit distribution and the fitted model. Optimization was performed using lsqnonlin with a MultiStart (MATLAB Global Optimization Toolbox), using 50 initial guesses to ensure robustness and convergence to the global minimum to avoid local minima;
- $F_0(t)$ and $F_{3/2}(t_s)$ are the Greenwood–Williamson functions defined as:

$$F_0(t) = \int_t^{\infty} \Phi(z)dz \tag{8}$$

$$F_{3/2}(t_s) = \int_{t_s}^{\infty} (z - t_s)^{3/2}\Phi_s(z)dz \tag{9}$$

where

$$t = \frac{d}{\tilde{\sigma}} \tag{10}$$

is the normalized gap distance between rubber and substrate, with d the actual gap determined by the equilibrium condition for contact pressure, and $\tilde{\sigma}$ is the standard deviation of $\Phi(z)$. d was determined by numerically solving the non-linear contact

balance derived from GW theory. The force balance equation includes the mechanical response of asperities and their deformation under pressure p and depends on the viscoelastic modulus of the rubber, which is dynamically adapted based on temperature and frequency. The solution was obtained using fsolve, starting from an initial guess and using suitable optimization tolerances. Similarly

$$t_s = \frac{d_s}{\tilde{\sigma}_s} \tag{11}$$

where d_s and $\tilde{\sigma}_s$ are the corresponding parameters for the summit height distribution $\Phi_s(z)$. Both the integrals were numerically evaluated using quadrature-based integration (integral function). The integration bounds are derived from the normalized separation presented above;

- $\tilde{n}_s$ represents the actual number of points of contact [63], evaluated as:

$$\tilde{n}_s = 6\pi\sqrt{3}\lambda_c^2 n_s \tag{12}$$

where $\lambda_c \sim 10^{-10}$ m is the lowest possible contact length, and n_s is the microscopic summit density:

$$n_s = \frac{m_4}{6\pi\sqrt{3}m_2} \tag{13}$$

Here, m_2 and m_4 represent the second and fourth moments of spectrum of the detrended surface profiles, computed via a gradient based method:

$$m_2 = \left\langle \left(\frac{dz}{dx}\right)^2 \right\rangle \qquad m_4 = \left\langle \left(\frac{d^2z}{dx^2}\right)^2 \right\rangle; \tag{14}$$

This step ensures consistency with the original GW framework which relies on these moments to statistically characterize surface asperities;

- D_m and D_M come from analyzing the slopes of the HDC function in two different scaling regimes (Section 2.2);
- λ_x is the crossing point of the two scales (Section 2.2);

Based on Eq. (6), λ_{min} is evaluated with a numerical optimization process designed for solving systems of nonlinear equations by using the fsolve function. The optimization method iteratively refines estimates of λ_{min} to minimize the difference between calculated and expected values. This approach takes into account various tire operating conditions, including sliding velocity, surface temperature and contact pressure, alongside the tire's viscoelastic properties shifted using the time–temperature superposition principle (WLF-type approach).

Once λ_{min} is established, the ratio A_c/A_0 of the actual contact area to the nominal area follows from the analytical expression:

$$\frac{A_c}{A_0} \approx \left(\frac{\xi_{\parallel} F_0^2(t) F_{3/2}(t_s) |E^*(2\pi v/\xi_{\parallel})| \tilde{n}_s^2}{808\pi s^{3/2} \xi_{\perp} |E^*(2\pi v/\lambda_{min})|} \right)^{\frac{1}{3}} \tag{15}$$

While it is clear from the formulas (15) and (6) how the roughness data and viscoelastic properties enter the model, it is important to underline that the sliding velocity, contact pressure and tire temperature are needed as well. In particular, the sliding velocity v of the tire on the rough surface and the surface temperature of the tire T_{surf} are essential to evaluate the frequencies $2\pi v/\lambda$ and temperatures to which the storage modulus and loss factor correspond (viscoelastic master curves shifting), while the contact pressure p is needed to evaluate properly, though a numerical optimization, the separation d between the free surface of the rubber and the mean plane of the counter rough surface. Hence, it becomes clear that it is possible to obtain the A_c/A_0 from the model as a function of p, T_{surf}, v.

An illustration of a road profile, highlighting its spherical macro-asperities along with the indentation depth of the rubber on the rough surface, d, is presented in Fig. 11(a). Additionally, the height and summit distributions used for the numerical assessment of the s parameter are shown in Fig. 11(b).

For what concerns the outdoor analysis, given the roughness data of each track (Section 2), and the viscoelastic properties of the compound (Section 3), the extended GW model was employed to perform various simulations. The resulting A_c/A_0 ratio (Eq. (15)), with a constant sliding velocity v, is illustrated in Fig. 12 as a function of T_{surf} and p for each track. All results related to the outdoor environment are presented without numerical values for confidentiality purposes.

It can be observed that the model responds consistently to variations in both temperature and contact pressure. Specifically, as the temperature increases, the compound exhibits a softer behavior, resulting in a larger contact area and, consequently, a higher A_c/A_0 ratio. A similar effect is related to the contact pressure since an increase of it leads to an higher level of indentation and thus an higher A_c/A_0 ratio. A classification among the tracks is observable as well as track 5 and 4 have the highest A_c/A_0, track 3 shows a middle level of A_c/A_0 and tracks 2 and 1 present the lowest A_c/A_0 for all the conditions.

The consideration regarding the coherency of the model output can be better observable from Fig. 13 where the A_c/A_0 ratio, simulated again with a constant sliding velocity, is reported as a function of T_{Surf} for different values of pressure, in particular $p_1 < p_2 < p_3 < p_4 < p_5$. Indeed an increase with both temperature and contact pressure is observable together with a saturation effect by increasing the contact pressure.

In the indoor environment, model simulations were performed at three distinct temperatures (25, 45, 70 °C) and three contact pressures (100, 150 and 200 kPa), using a fixed sliding velocity for the reference compound. The resulting A_c/A_0 values, plotted as function of surface temperature (T_{surf}) and contact pressure (p) for each road specimen considered in this study, are presented in Fig. 14.

The model continues to show consistent responses under variations in both temperature and contact pressure. Notably, roads 5 and 4 exhibit the highest A_c/A_0 ratios, road 3 displays an intermediate level, and roads 2 and 1 consistently yield the lowest A_c/A_0 values for all tested conditions.

Moreover, the analysis was extended to two sandpaper surfaces with different grit sizes. This choice was made to challenge the model with a distinctly unique surface texture and thus represent a more unconventional interaction setting for the tire-surface system.

The A_c/A_0 simulations as a function of pressure and temperature, along with the sandpapers, are shown in Fig. 15. It can be observed that, while the overall trend with tire temperature and contact pressure remains consistent, the sandpapers exhibit a globally higher A_c/A_0 ratio compared to the road specimens, due to their distinctive surface texture. Indeed, it is noticeable that the sandpapers are on another level compared to the road specimens as by adding the simulated A_c/A_0 for the sandpapers on the plot, the difference among the roads is not as observable anymore. This is representative of another category of surfaces, aligning with the high difference in terms of texture presented in Fig. 1.

5. Friction analysis

The contact model was used to estimate the A_c/A_0 ratio by considering a specific compound, whose viscoelastic properties are reported in Section 3. This compound was used as a reference for both indoor and outdoor friction testing campaigns. In particular, regarding the indoor environment, the friction tester used for this research activity was the Evolved British Pendulum of the University of Naples Federico II [64] and all the tests were performed on five different road specimens and two sandpapers, whose roughness characteristics have been presented in Section 2. Differently, the outdoor testing campaign was performed with a high-performance vehicle properly equipped with various sensors and the tests were performed on five different tracks, whose roughness properties have been presented in Section 2.

The aim of both the indoor and outdoor testing campaigns was to evaluate the experimental maximum friction and correlate this quantity with the simulated A_c/A_0 ratio.

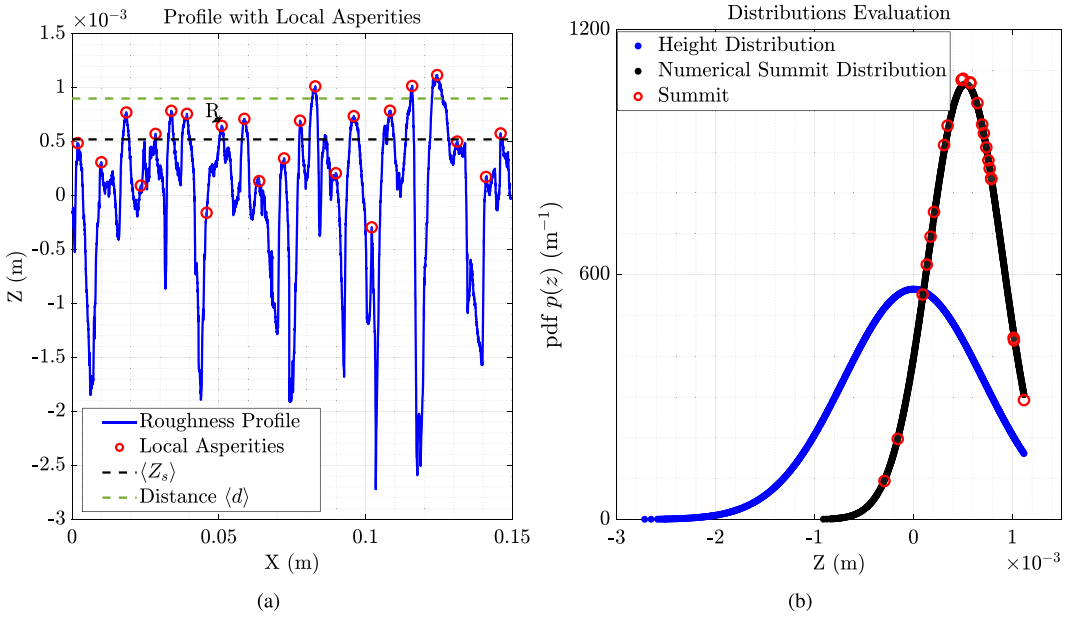

Fig. 11. Road profile analysis: (a) spherical macro asperities and level of indentation of the rubber on the rough substrate, (b) height and peaks distribution for the numerical evaluation of the s parameter.

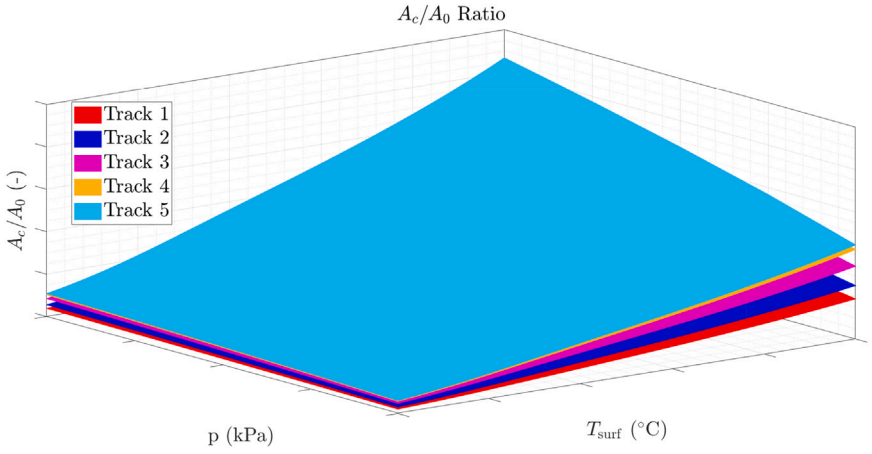

Fig. 12. A_c/A_0 simulation as a function of pressure and temperature for each track.

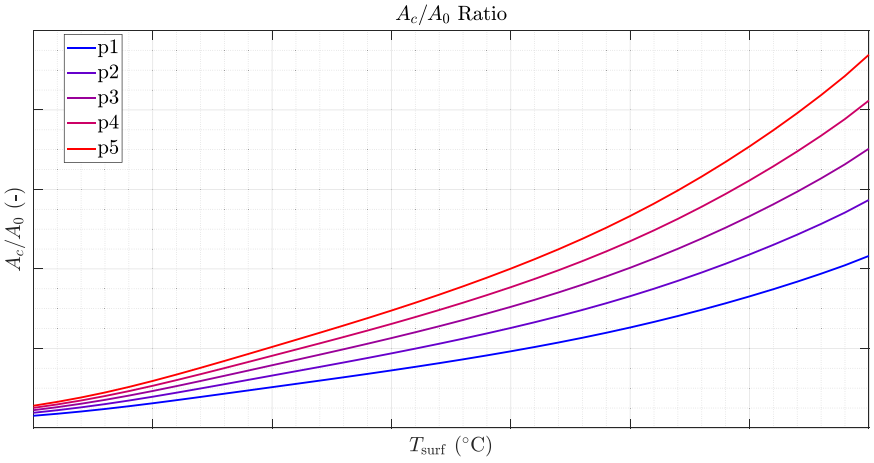

Fig. 13. A_c/A_0 trend for different pressures as a function of the surface temperature - Track 1.

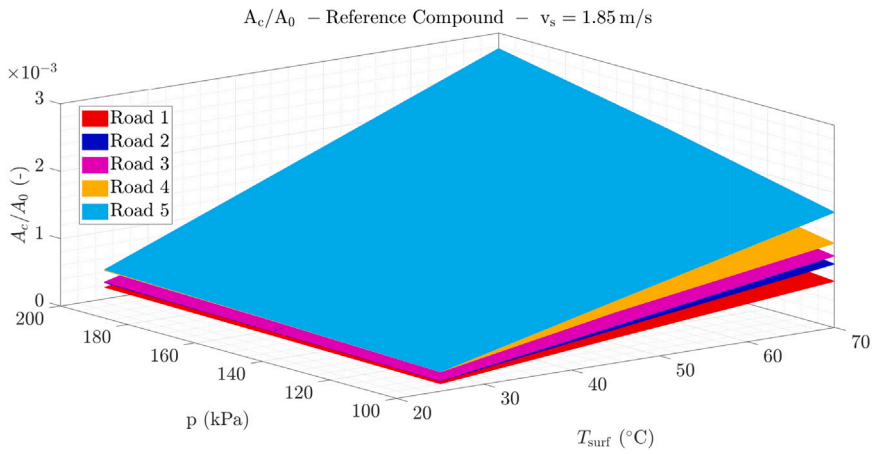

Fig. 14. A_c/A_0 simulation as a function of pressure and temperature for each road specimen and for the reference compound.

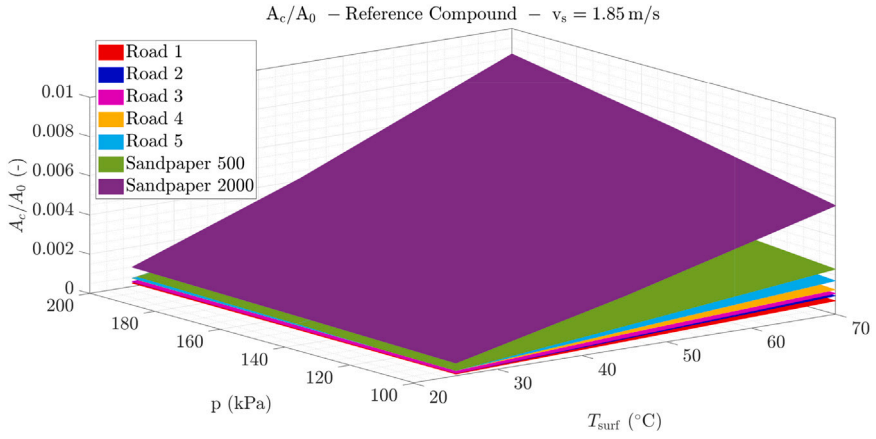

Fig. 15. A_c/A_0 simulation as a function of pressure and temperature for each road specimen and sandpapers and for the reference compound.

5.1. Outdoor testing campaign

The outdoor testing campaign refers to a high-performance vehicle instrumented with a range of sensors and all the tests were carried out with the same compound on five different tracks. The acquired data was used to conduct a friction analysis and a comparison of the performance of the tire compound across each track. The aim of the research activity was to correlate the simulated A_c/A_0 ratio with the corresponding experimental friction values exhibited with the same compound, road roughness and tire operating conditions.

The first step consists of extracting the friction values for each track based on the acquired telemetry data. The tire friction coefficient by definition is evaluated as:

$$\mu = \frac{F_t}{F_z} \tag{16}$$

where F_t is the tangential force and F_z is the vertical load acting on the tire. From this equation, it is thus possible to evaluate the longitudinal grip μ_x by considering the longitudinal component of the tangential forces F_x, and the lateral grip μ_y by considering the lateral component of the tangential forces F_y.

In particular, for this research activity, the attention was mainly posed on the pure lateral interaction within the so-called grip-limited zones which correspond to the highest friction conditions. Defining grip-limited zones as areas of interest proved useful, as it reduced the amount of collected data while focusing on conditions where the car exhibits high levels of grip. Indeed, achieving high grip values is a key to increase both tire performance and road safety.

The theory of grip limited involves identifying all the conditions under which it is possible to establish a narrow region of friction values close to the border of the adherence ellipse [65]. In this way, only the regions associated with high grip values were considered, while those with low grip were excluded as they are less relevant for studying vehicle performance. Additionally, it is important to note that the loss of lateral grip is more critical than the loss of longitudinal grip, making the study of lateral adherence essential for understanding tire behavior.

To identify the pure lateral interaction, a series of thresholds have been defined on the data, in particular on the slip ratio, tire sideslip angle, longitudinal acceleration, lateral acceleration, longitudinal velocity, vertical load and surface temperature channels. The lateral friction coefficient versus slip angle plot for the rear axle, obtained from the experimental friction testing campaign using the reference compound, is shown in Fig. 16. This figure also displays the data related to the five different tracks.

Starting from the relationship between lateral friction coefficient and slip angle, it is possible to obtain the lateral interaction curve and by evaluating the peak of this curve, the maximum attainable friction coefficient can be determined. An envelope curve was then implemented to optimize the representation of the acquired data, enhancing the accuracy and reliability of the resulting point cloud representation. The envelope curve was determined through a mathematical optimization process to accurately represent the experimental data. To ensure robustness and reliability, multiple local maxima were identified across the data, and an average was computed to define the reference maximum friction coefficient. This approach minimizes the impact of

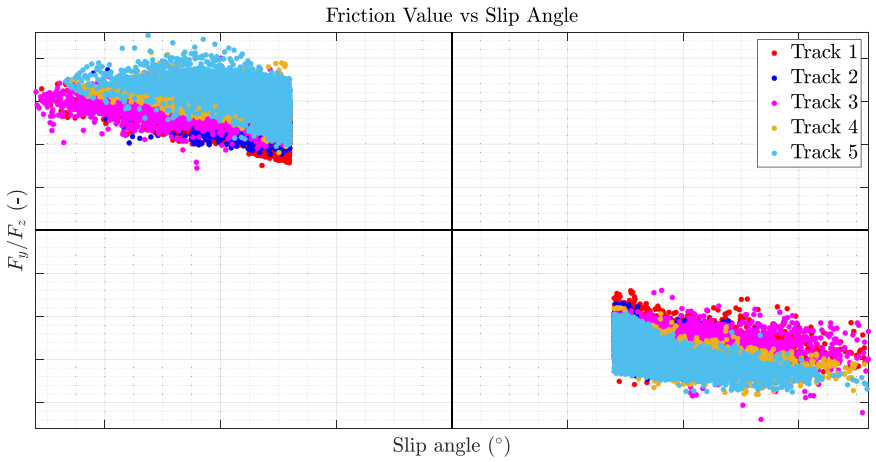

Fig. 16. Friction - Slip angle relationship: experimental points for each track.

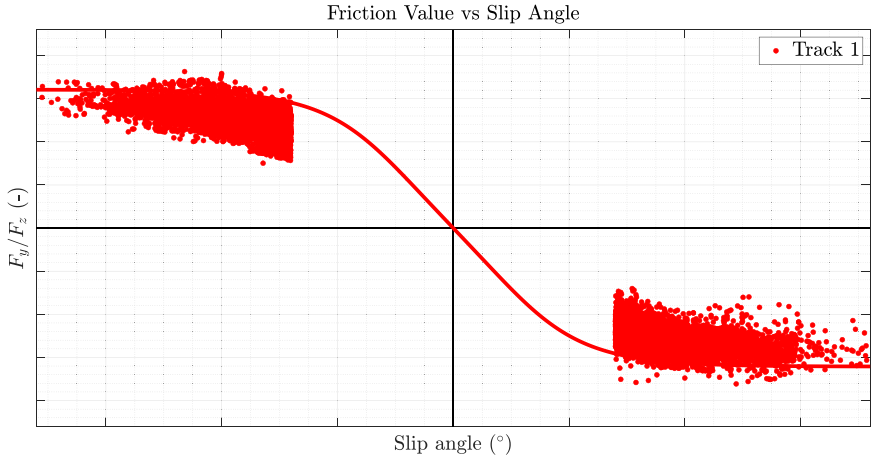

Fig. 17. Friction - Slip angle: experimental points and envelope lateral curve for track 1.

outliers and noise, providing a consistent representation of the maximum achievable grip, which serves as an indicator of tire performance and road adherence.

This procedure was performed for each track, and the maximum friction coefficient extracted from the lateral interaction curve is representative of the maximum friction conditions achieved for that track. An example of the envelope curve related to the telemetry data obtained from track 1 for the rear axle is shown in Fig. 17, which also represents the enveloped experimental points.

The maximum friction values obtained for each track are detailed in the bar diagram shown in Fig. 18. It is noticeable that, under the best tire operating conditions characteristic of each track, the highest friction is achieved on tracks 4 and 5, track 3 has a medium level of friction, and the lowest friction is obtained on tracks 1 and 2.

5.2. Indoor testing campaign

The indoor friction testing campaign was carried out by considering the road specimens and the same compound presented in Section 4, regarding the A_c/A_0 simulations for the indoor environment. The friction tester used in this research is an evolution of the British Pendulum, enhanced with additional sensors, from the University of Naples Federico II (Fig. 19).

It is equipped with a triaxial load cell and an encoder to measure the tangential and normal forces developed during contact between the rubber and the asphalt test specimen, as well as the velocity of the pendulum arm. This allows for the evaluation of the friction coefficient μ by analyzing the signals resulting from the measurement that are recorded using an analog-to-digital converter and processed in an appropriate computing environment. The pendulum is supported by a robust structure designed to provide stability and allow proper positioning of the workbench. The testing bench has an oscillating arm which incorporates a pre-loading spring and a lever system to ensure consistent contact pressure between the rubber test specimen and the road surface during sliding. Additionally, a pre-loading mass is included to increase the inertia of the arm once the mechanism is activated.

The structure includes a graduated crown, which is used to identify the angular position of the arm relative to the axis passing through the center of oscillation and parallel to the workbench. An encoder is also integrated to measure the oscillation velocities accurately. The rubber specimen, shaped as a parallelepiped is located in the tread specimen holder using a specialized adhesive resistant to high mechanical and thermal stresses. The base also includes a robust mounting system to hold the road test specimens during experiments, with a load cell positioned underneath to measure the forces generated during testing.

To establish a relationship between the friction measurements and the simulated A_c/A_0 ratio, tests were conducted under controlled tire temperature and sliding velocity conditions, mirroring those used in the contact model described in Section 4. Fig. 20 presents the friction outcomes obtained from the indoor testing campaign on the five road specimens and on two sandpapers (each with a different grit size), all evaluated using the same compound.

For what concerns the roads, it is possible to notice that for all the testing conditions, roads 5 and 4 are high-friction roads, road 3 has

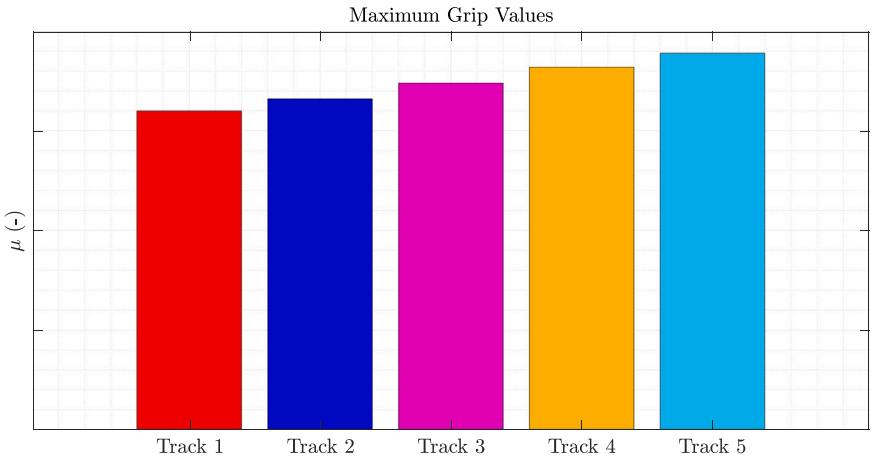

Fig. 18. Maximum grip values for each track.

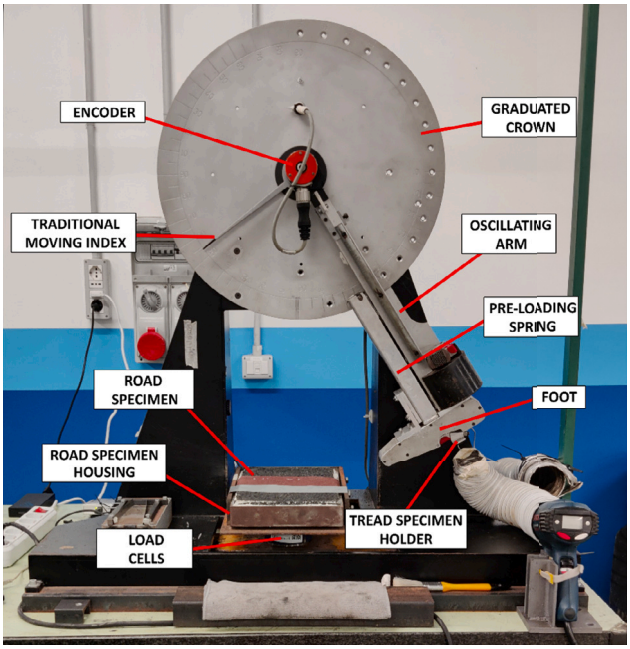

Fig. 19. British pendulum evolved.

a medium level of friction, and roads 2 and 1 are representative of low-friction surfaces.

Moreover, as previously noted, the analysis of the two sandpapers with different grain sizes aimed to enhance the reliability of the results by incorporating an unconventional scenario, specifically the interaction between tires and sandpapers.

By analyzing the results on the tested sandpapers, it is observable that they are still coherent and robust since the obtained friction levels for the sandpapers are globally higher and different if compared to the road specimens, due to their peculiarity and singularity in terms of surface texture.

6. Discussion

Based on the analysis of the simulated A_c/A_0 ratios and the experimental friction values, it is noteworthy that the ranking of the simulated A_c/A_0 ratios matches that of the maximum friction values in both outdoor and indoor environments.

For what concerns the outdoor, this can be clearly observed by comparing Fig. 12 reporting the simulated A_c/A_0 ratio for each track and Fig. 18 in which the experimental friction values for each track are reported. A clear correlation emerges between the friction measurements and the model's predicted A_c/A_0 ratio: higher friction values align with larger A_c/A_0, whereas lower friction values correspond to smaller A_c/A_0. Indeed, combining the friction values classification and the A_c/A_0 ratio ranking within the same table highlights a clear correlation between the two quantities. This is evident in the Table 3 in which the classification of the A_c/A_0 ratio and friction values from the highest to the lowest with respect to the track is presented. The values reported in the table are for a single condition but the relationship is valid for all the combinations.

Table 3
Classification of the A_c/A_0 ratio (values reported for T_{surf} = 70 °C, p = 100 kPa and v_s = 1.85 m/s) and friction values from the highest to the lowest with respect to the track.

Ranking	Friction coefficient	A_c/A_0
1°	Track 5	4.45E−04 for Track 5
2°	Track 4	4.42E−04 for Track 4
3°	Track 3	3.44E−04 for Track 3
4°	Track 2	2.25E−04 for Track 2
5°	Track 1	1.89E−04 for Track 1

Interestingly, this evidence suggests a strong correlation between the A_c/A_0 ratio and the experimental friction coefficient: by considering the same compound and simulating A_c/A_0 ratio for a specific surface, a high A_c/A_0 ratio corresponds to high grip track and vice versa.

Moreover, as observed for the outdoor environment, even in the indoor one it is possible to state the classification of the simulated A_c/A_0 ratio for each road specimen is the same as that of the experimental grip values in the same operating conditions. This can be clearly observed by comparing Fig. 14, which reports the simulated A_c/A_0 ratio for each road specimen, with Fig. 20, which presents the experimental friction values for the same specimens, using the same tire compound and operating conditions. In addition, this observation holds even when considering specific scenarios involving sandpapers with unique surface textures. By comparing the simulated A_c/A_0 ratio presented in Fig. 15 with the experimental friction values shown in Fig. 20, it is evident again that a higher A_c/A_0 ratio leads to a higher experimental friction coefficient.

A summary of the grip value classification and the simulated A_c/A_0 ratio ranking for the various surfaces considered in the indoor environment is provided in Table 4. The table presents the classification of both A_c/A_0 ratios and friction values, from highest to lowest,for road specimens and sandpapers, once again highlighting a clear correlation between the two quantities. Also in this case, the values reported in the

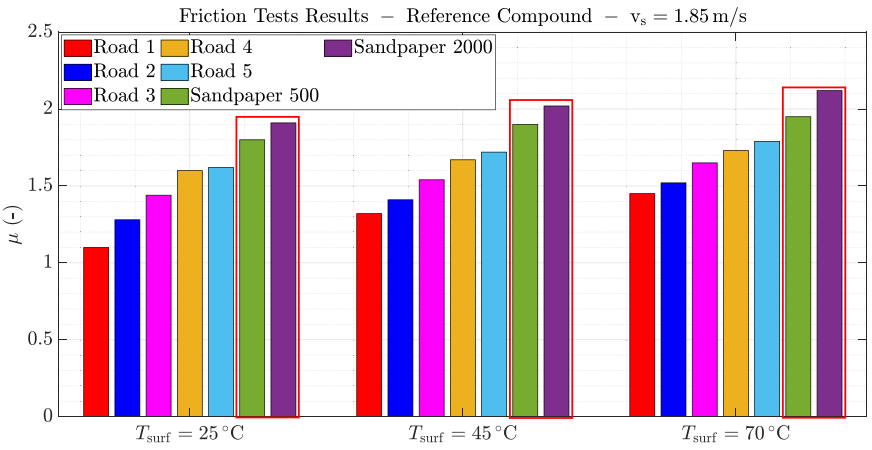

Fig. 20. Friction tests results on both road specimens and sandpapers from the British Pendulum evolved for the reference compound.

Table 4
Classification of the A_c/A_0 ratio (values reported for T_{surf} = 70 °C, p = 100 kPa and v_s = 1.85 m/s) and friction values (values reported for T_{surf} = 70 °C and v_s = 1.85 m/s) from the highest to the lowest with respect to the road specimens and sandpapers.

Ranking	Friction coefficient	A_c/A_0
1°	2.12 for Sandpaper 2000	5.54E−03 for Sandpaper 2000
2°	1.95 for Sandpaper 500	2.30E−03 for Sandpaper 500
3°	1.79 for Road Specimen 5	1.71E−03 for Road Specimen 5
4°	1.73 for Road Specimen 4	1.25E−03 for Road Specimen 4
5°	1.65 for Road Specimen 3	1.06E−03 for Road Specimen 3
6°	1.52 for Road Specimen 2	9.41E−04 for Road Specimen 2
7°	1.45 for Road Specimen 1	6.86E−04 for Road Specimen 1

table are for a single condition but the relationship is valid for all the combinations.

The presented results clearly demonstrate that the simulated A_c/A_0 values consistently align with the experimental friction measurements. This correlation is significant: higher friction surfaces correspond to higher A_c/A_0 values predicted by the model, while lower friction surfaces yield lower A_c/A_0 values. Additionally, whenever two surfaces produce similar friction levels, the model predicts comparable A_c/A_0 values under the same conditions. This consistent relationship underscores the reliability of the model and its effectiveness in predicting friction behavior, highlighting its potential utility in real-world applications.

7. Conclusions

In this paper, a physical-analytical contact model was developed to predict tire-road interaction by analyzing road roughness, tire viscoelasticity, and tire operating conditions through the A_c/A_0 ratio. Notably, it showed a strong relationship between the A_c/A_0 ratio and experimental friction values at the same operating conditions. The consistency of the results is evident in both outdoor environments, where a properly equipped high-performance vehicle on five different tracks was considered, and indoor settings, where the tests were conducted under controlled conditions using the British Pendulum evolved as friction tester on seven different surfaces, including two sandpapers with different granulometry to explore unconventional scenarios to validate the results. Despite the higher friction coefficients exhibited by the sandpapers compared to road surfaces, the model consistently predicts a greater real contact area.

In both environments, the classification of the experimental grip values aligns properly with the classification of the simulated A_c/A_0 across the various surfaces. This physical-analytical approach closely correlates with the experimental friction values expected on a given surface. Such analysis supports the evaluation of expected friction levels in tire-road interactions, with direct implications for road safety. It is also beneficial in motorsport, enabling performance analysis in virtual environments to maximize grip on track according to the selected tire compound.

Furthermore, this ratio is significantly affected by the roughness of the road surface, the tire's viscoelastic properties and its operating conditions. This forms the basis for further analysis on these topics and lays the groundwork for a comprehensive friction analysis. Indeed, starting from the results obtained and reported in this paper, further developments will focus on implementing of a physical friction model, that leverages the observed correlation between variables (friction coefficient and A_c/A_0) to predict friction maps for specific roads with reference to specific tire compounds.

CRediT authorship contribution statement

Flavio Farroni: Writing – review & editing, Supervision, Project administration, Methodology, Funding acquisition, Formal analysis, Conceptualization. **Raffaele Stefanelli:** Writing – original draft, Visualization, Validation, Software, Methodology, Formal analysis, Data curation. **Guido Napolitano Dell'Annunziata:** Writing – original draft, Validation, Software, Resources, Methodology, Investigation, Data curation. **Francesco Timpone:** Writing – review & editing, Visualization, Supervision, Resources, Project administration, Funding acquisition, Conceptualization.

Funding

This work was partly supported by the project "FINGERTIPS - Friction-Increase Nanopoles and Grooves Exploitation in Road-Tire Interaction for Preventive Safety" funded by the Italian MUR "Progetti di Ricerca di Rilevante Interesse Nazionale (PRIN 2022 PNRR PE8)"– grant n. P2022LZWF5 - P.I. Flavio Farroni.

Declaration of competing interest

The authors declare that they have no known competing financial interests or personal relationships that could have appeared to influence the work reported in this paper.

Data availability

The data that has been used is confidential.

References

[1] Kane Malal, Edmondson Vikki. Tire/road friction prediction: Introduction a simplified numerical tool based on contact modelling. Veh Syst Dyn 2022;60(3):770–89.
[2] Johnson Kenneth Langstreth, Johnson Kenneth Langstreth. Contact mechanics. Cambridge University Press; 1987.
[3] Persson Bo NJ. Theory of rubber friction and contact mechanics. J Chem Phys 2001;115(8):3840–61.
[4] Persson Bo NJ, Albohr Oliver, Tartaglino Ugo, Volokitin Aleksandr Ivanovich, Tosatti Erio. On the nature of surface roughness with application to contact mechanics, sealing, rubber friction and adhesion. J Phys: Condens Matter 2004;17(1):R1.
[5] Le Gal André, Klüppel Manfred. Investigation and modelling of rubber stationary friction on rough surfaces. J Phys: Condens Matter 2007;20(1):015007.
[6] Klüppel Manfred, Heinrich Gert. Rubber friction on self-affine road tracks. Rubber Chem Technol 2000;73(4):578–606.
[7] Persson Bo NJ, Tosatti Erio. Physics of sliding friction, vol. 311, Springer Science & Business Media; 2013.
[8] Costa Henara Lillian, Cousseau Tiago, Souza Roberto Martins. Current knowledge on friction, lubrication, and wear of ethanol-fuelled engines—A review. Lubricants 2023;11(7):292.
[9] Alvarez Luis, Yi Jingang, Horowitz Roberto, Olmos Luis. Dynamic friction model-based tire-road friction estimation and emergency braking control. 2005.
[10] Hertz Heinrich. Ueber die berührung fester elastischer körper. 1882.
[11] Popov Valentin L, et al. Contact mechanics and friction. Springer; 2010.
[12] Suphadon N, Thomas AG, Busfield JJC. Viscoelastic behavior of rubber under a complex loading. J Appl Polym Sci 2009;113(2):693–9.
[13] Popov Valentin L, Heß Markus, Willert Emanuel. Handbook of contact mechanics: exact solutions of axisymmetric contact problems. Springer Nature; 2019.
[14] Bhushan Bharat. Contact mechanics of rough surfaces in tribology: multiple asperity contact. Tribol Lett 1998;4:1–35.
[15] Sofonea Mircea, Matei Andaluzia. Mathematical models in contact mechanics. Cambridge University Press; 2012, Number 398.
[16] Bowden Frank Philip, Tabor David. The area of contact between stationary and moving surfaces. Proc R Soc Lond Ser A Math Phys Sci 1939;169(938):391–413.
[17] Ghaednia Hamid, Wang Xianzhang, Saha Swarna, Xu Yang, Sharma Aman, Jackson Robert L. A review of elastic–plastic contact mechanics. Appl Mech Rev 2017;69(6):060804.
[18] Archard JeFoa. Contact and rubbing of flat surfaces. J Appl Phys 1953;24(8):981–8.
[19] Archard JF. Elastic deformation and the laws of friction. Proc R Soc Lond Ser A Math Phys Sci 1957;243(1233):190–205.
[20] Sneddon Ian N. The relation between load and penetration in the axisymmetric Boussinesq problem for a punch of arbitrary profile. Internat J Engrg Sci 1965;3(1):47–57.
[21] Greenwood James A, Williamson JB Pl. Contact of nominally flat surfaces. Proc R Soc Lond Ser A Math Phys Sci 1966;295(1442):300–19.
[22] Bush AW, Gibson RD, Thomas TR. The elastic contact of a rough surface. Wear 1975;35(1):87–111.
[23] Jackson Robert L, Green Itzhak. On the modeling of elastic contact between rough surfaces. Tribol Trans 2011;54(2):300–14.
[24] Eid Hassan, Pamp Andy. An introductory overview of contact mechanics and adhesion. 2006.
[25] Johnson Kenneth Langstreth, Kendall Kevin, Roberts aAD. Surface energy and the contact of elastic solids. Proc R Soc A 1971;324(1558):301–13.
[26] Derjaguin Boris V, Muller Vladimir M, Toporov Yu P. Effect of contact deformations on the adhesion of particles. J Colloid Interface Sci 1975;53(2):314–26.
[27] Tabor D. Surface forces and surface interactions. In: Plenary and invited lectures. Elsevier; 1977, p. 3–14.
[28] Muller VM, Yushchenko VS, Derjaguin BV. On the influence of molecular forces on the deformation of an elastic sphere and its sticking to a rigid plane. J Colloid Interface Sci 1980;77(1):91–101.
[29] Maugis Daniel. Adhesion of spheres: the JKR-dmt transition using a dugdale model. J Colloid Interface Sci 1992;150(1):243–69.
[30] Persson BNJ. Adhesion between an elastic body and a randomly rough hard surface. Eur Phys J E 2002;8:385–401.
[31] Persson Bo NJ. Contact mechanics for randomly rough surfaces. Surf Sci Rep 2006;61(4):201–27.
[32] Heinrich Gert, Klüppel Manfred. Rubber friction, tread deformation and tire traction. Wear 2008;265(7–8):1052–60.
[33] Müser Martin H, Nicola Lucia. Modeling the surface topography dependence of friction, adhesion, and contact compliance. MRS Bull 2022;47(12):1221–8.
[34] Sayers MW, Gillespie TD, Queiroz CAV. The international road roughness experiment: A basis for establishing a standard scale for road roughness measurements. Transp Res Rec 1986;1084:76–85.
[35] Pegram Megan Savannah, Tavernini Davide, Gruber Patrick. Obtaining rubber friction characteristics from flat-track tire testing. In: International symposium on advanced vehicle control. 2022.
[36] Jacobs Tevis DB, Junge Till, Pastewka Lars. Quantitative characterization of surface topography using spectral analysis. Surf Topogr: Metrol Prop 2017;5(1):013001.
[37] Sun Lu, Zhang Zhanming, Ruth Jessica. Modeling indirect statistics of surface roughness. J Transp Eng 2001;127(2):105–11.
[38] Kienle Rebekka, Ressel Wolfram, Götz Tobias, Weise Markus. The influence of road surface texture on the skid resistance under wet conditions. Proc Inst Mech Eng Part J: J Eng Tribol 2020;234(3):313–9.
[39] D'Agostino Vincenzo. Fondamenti di tribologia. Cooperativa universitaria editrice napoletana; 1984.
[40] Gadelmawla Elamir S, Koura Monir M, Maksoud Talal MA, Elewa Ibrahiem M, Soliman Hassan H. Roughness parameters. J Mater Process Technol 2002;123(1):133–45.
[41] Torbruegge Stefan, Wies Burkhard. Characterization of pavement texture by means of height difference correlation and relation to wet skid resistance. J Traffic Transp Eng (Engl Ed) 2015;2(2):59–67.
[42] Goryacheva IG, Makhovskaya Yu Yu. Modeling of friction at different scale levels. Mech Solids 2010;45:390–8.
[43] Heinrich Gert. Hysteresis friction of sliding rubbers on rough and fractal surfaces. Rubber Chem Technol 1997;70(1):1–14.
[44] Yun Di, Sha Aimin, Hu Liqun, Tang Cheng, Gao Jie. Laboratory study on the relationship between pavement texture and tread rubber penetration depth. Int J Pavement Eng 2022;23(5):1645–58.
[45] Vanormelingen K, Degroote B, Vantomme A. Quantitative characterization of the surface morphology using a height difference correlation function. J Vac Sci Technol B: Microelectron Nanometer Struct Process Meas Phenom 2006;24(2):725–9.
[46] Heinrich G, Klüppel M, Vilgis Thomas A. Evaluation of self-affine surfaces and their implication for frictional dynamics as illustrated with a rouse material. Comput Theor Polym Sci 2000;10(1–2):53–61.
[47] Lakes Roderic S. Viscoelastic materials. Cambridge University Press; 2009.
[48] Mark James E, Erman Burak, Roland Mike. The science and technology of rubber. fourth ed.. Academic Press; 2013.
[49] Matsumoto Takayoshi, Segawa Yasuhiko, Warashina Yoshiro, Onogi Shigeharu. Nonlinear behavior of viscoelastic materials. II. The method of analysis and temperature dependence of nonlinear viscoelastic functions. Trans Soc Rheol 1973;17(1):47–62.
[50] Glöckle WG, Nonnenmacher Th F. Fractional relaxation and the time-temperature superposition principle. Rheol Acta 1994;33:337–43.
[51] Povolo F, Fontelos M. Time-temperature superposition principle and scaling behaviour. J Mater Sci 1987.
[52] Montes Helene, Lequeux Francois, Berriot Julien. Influence of the glass transition temperature gradient on the nonlinear viscoelastic behavior in reinforced elastomers. Macromolecules 2003;36(21):8107–18.
[53] Menard Kevin P, Menard Noah R. Dynamic mechanical analysis. CRC Press; 2020.
[54] Cho Kwang Soo. Theory of linear viscoelasticity. In: Viscoelasticity of polymers. Springer; 2016.
[55] Genovese Andrea, Maiorano Antonio, Russo Riccardo. A novel methodology for non-destructive characterization of polymers' viscoelastic properties. Int J Appl Mech 2022;14(03):2250017.
[56] Genovese Andrea, Pastore Sebastian Rosario. Development of a portable instrument for non-destructive characterization of the polymers viscoelastic properties. Mech Syst Signal Process 2021;150:107259.
[57] Ferry JD. Viscoelastic properties of polymers, vol. 264, Wiley; 1980.
[58] Dagdug L, García-Colín LS. Generalization of the Williams–Landel–Ferry equation. Phys A 1998;250(1–4):133–41.
[59] Lang Andrej, Klüppel Manfred. Influences of temperature and load on the dry friction behaviour of tire tread compounds in contact with rough granite. Wear 2017;380:15–25.
[60] Pawar Gorakh, Pawlus Pawel, Etsion Izhak, Raeymaekers Bart. The effect of determining topography parameters on analyzing elastic contact between isotropic rough surfaces. J Tribol 2013;135(1):011401.
[61] Tomanik Eduardo, Chacon Haroldo, Teixeira Giovanni. A simple numerical procedure to calculate the input data of greenwood-williamson model of asperity contact for actual engineering surfaces. In: Tribology series. vol. 41, Elsevier; 2003, p. 205–15.
[62] Klüppel M, Müller A, Le Gal A, Heinrich G, Continental AG. Dynamic contact of tires dynamic contact of tires with road tracks with road tracks. 2003.
[63] McCool John I. Relating profile instrument measurements to the functional performance of rough surfaces. 1987.
[64] Ciaravola Vincenzo, Farroni Flavio, Fortunato Gaetano, Russo Michele, Russo Riccardo, Sakhnevych Aleksandr, Timpone Francesco. An evolved version of the british pendulum tester for the experimental investigation of contact between tire tread and rough surfaces. Eng Lett 2017;25(1).
[65] Brach Raymond, Brach Matthew. The tire-force ellipse (friction ellipse) and tire characteristics. Technical report, SAE Technical Paper; 2011.